Solid-State Near-Edge X-ray Absorption Fine Structure Spectra of Glycine in Various Charge States

Yan Zubavichus,*,†,‡ Andrey Shaporenko,† Michael Grunze,† and Michael Zharnikov*,†

Angewandte Physikalische Chemie, University of Heidelberg, INF 253, 69120 Heidelberg, Germany, and Institute of Organoelement Compounds, Russian Academy of Sciences, 28 Vavilova st., 119991 Moscow, Russia

Received: October 25, 2005; In Final Form: January 4, 2006

The experimental solid-state near-edge X-ray absorption fine structure spectra for a series of glycine-related samples including α-glycine, *β*-glycine, glycinium chloride, glycinium trifluoroacetate, and sodium glycinate at the C, N, and O K-edges measured under identical conditions are reported and compared. An assignment of spectral features for α-glycine is proposed on the basis of extended theoretical simulations of polarization-dependent spectra performed within the real-space multiple-scattering formalism explicitly taking into account the intermolecular environment of a glycine molecule in a crystal.

1. Introduction

Glycine is the simplest and one of the most abundant amino acids constituting proteins. Furthermore, it is one of the smallest organic molecules that is solid under normal conditions. Isolated glycine molecules in the gas phase are neutral but intermolecular interactions occurring in the condensed state favor proton transfer from the carboxy group to the amino group giving rise to the glycine zwitterion. The resultant dipole−dipole interactions and H-bonds are so strong that glycine, which is characterized by a molecular mass as low as 75, melts with decomposition above 230−250 °C, which is rather typical of organic polymers.

Solid pristine glycine is known to exist in three polymorph modifications, viz., α-, *β*-, and *γ*-glycine, which somewhat differ from each other in the pattern of H-bonds formed by glycine zwitterions.[1−3] In aqueous solutions, three charge states of glycine, viz., zwitterion, glycinium cation, and glycinate anion coexist in equilibrium, with their mutual ratio being strongly dependent on pH of the solution. Acidic solutions are dominated by the glycynium cations, whereas it is the glycinate anions that prevail in basic solutions. The glycinium cation can easily be stabilized in the solid state in ionic salts of glycine with strong acids. The crystal structures of a variety of such salts (e.g., glycinium chloride, bromide, iodide, nitrate, sulfate, phosphate, arsenate, selenate, perchlorate, maleate, oxalate, trifluoroacetate, etc.) have been reported.[4−7] On the other hand, the glycinate anion can be stabilized through the coordination with metal cations. Complexes of the glycinate ligand with such metals as nickel, cobalt, copper, zinc, cadmium, silver, palladium, and platinum are known.[8,9] The bonding between the glycinate and metal atoms in such complexes is appreciably covalent. Structural information on more ionic salts of the glycinate anion is rather scarce. To our knowledge, only one such salt, lithium glycinate, has been characterized to date.[10] Sodium glycinate is available commercially, but it has not been prepared and studied as single crystals.

The molecular geometry adopted by the glycine molecules and the pattern of intermolecular bonds formed by them are naturally dependent on the charge state. In particular, two carboxylate oxygen atoms of glycine with the deprotonated carboxylate group (i.e., in the zwitterion and anion) are chemically equivalent, and thus the respective C−O bonds are equalized, becoming intermediate in length between typical single and double bonds.[1−3,10] In contrast, in the case of the protonated carboxy group that occurs in the cation, the C═O and C−OH bonds are substantially different in their lengths although the *π*-electron density is still appreciably delocalized over the two oxygen atoms.[4−7] Each glycine zwitterion in the crystal structure of the thermodynamically most stable phase of pristine glycine, α-glycine,[1] forms rather strong intermolecular N−H···O bonds with four neighboring zwitterions to build up layers in the crystallographic *ac* plane, as shown in the left panel of Figure 1. The layers are stacked together along the *b* axis through the substantially weaker bifurcated H-bonds. In the ionic salts of glycine, such as glycinium chloride or lithium glycinate, cation−anion interactions prevail so that no strong H-bonds are formed between neighboring glycine-derived ions. In particular, each chloride anion in the crystal structure of glycinium monochloride forms two N−H···Cl bonds and one O−H···Cl bond lying in the crystallographic *ab* plane (see central panel of Figure 1).[4] The lithium cations in the crystal structure of lithium glycinate are bonded to the lone pairs of three oxygen atoms and of one nitrogen atom in a nearly tetrahedral arrangement (see right panel of Figure 1).[10]

NEXAFS (near-edge X-ray absorption fine structure) spectroscopy is an approved tool in the elucidation of the electronic structure of organic substances.[11] Glycine has been a subject of several NEXAFS investigations.[12−23] Spectra of glycine vapor,[14,15] solution-cast[12−15] or vacuum-deposited[16−20] thin films, powder films,[21,22] and aqueous solutions[23] were reported and analyzed in combination with various theoretical calculations typically based on the geometric parameters of isolated glycine molecules as predicted by quantum-mechanical calculations.[13,14,18,23] Recently, the possible NEXAFS spectral effects of the glycine charge state and intermolecular environment have come into the focus of interest. In particular, Nyberg et al.[18] pointed out the importance of the formation of H-bonded dimers

* To whom correspondence should be addressed. E-mail: michael.zharnikov@urz.uni-heidelberg.de (M. Zharnikov) and Yan.Zubavichus@urz.uni-heidelberg.de (Y. Zubavichus)

† University of Heidelberg.

‡ Institute of Organoelement Compounds.

10.1021/jp056118p CCC: $33.50
Published on Web 01/28/2006

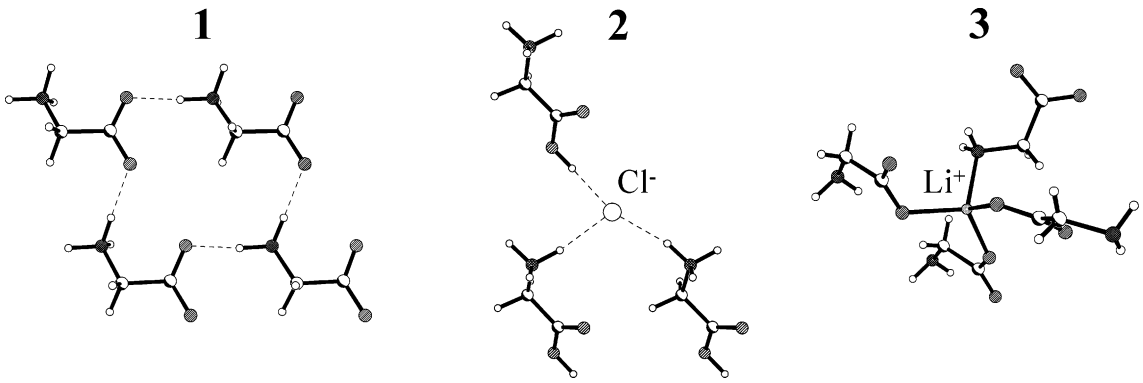

Figure 1. Fragments of the crystal structures of (**1**) α-glycine (projection in the *ac* plane), (**2**) glycinium chloride (projection in the *ab* plane), and (**3**) lithium glycinate (a random projection). Highlighted open circles denote carbon atoms, crosshatched circles denote oxygen atoms; diagonally shaded circles denote nitrogen atoms; small circles denote hydrogen atoms.

of glycinate ions on the Cu(110) crystal surface to explain specific features of the experimental symmetry-resolved NEXAFS spectra. Very recently, Messer et al.[23] observed variations of the NEXAFS spectra of glycine aqueous solutions as a function of pH.

In the present paper, we report on the experimental solid-state NEXAFS spectra of several samples of pristine glycine and related substances, such as glycinium chloride and sodium glycinate, measured under identical conditions using the partial electron yield mode. The experimental observations are supplemented by theoretical calculations for pristine zwitterionic α-glycine performed within the real-space multiple-scattering formalism based on the real experimental crystallographic data for this phase, which explicitly take into account both the molecular geometry and intermolecular environment of a glycine molecule.

2. Experimental Section

2.1. Sample Preparation for the NEXAFS Measurements. Samples of glycine and glycine-related substances suitable for the NEXAFS characterization were prepared in two ways. First, commercially available (Sigma-Aldrich Chemie GmbH, stated purity >98%) powders of pristine glycine (Gly), glycine hydrochloride (Gly^+ Cl^-), and sodium glycinate (Na^+ Gly^-) without any additional pretreatment were ground and pressed into clean indium foil. Afterward, the powder layers were carefully thinned with a brush. The resultant powder films were sufficiently thin to avoid charging, which is a prerequisite for the NEXAFS data collection using the electron yield. Meanwhile, the films were sufficiently thick to form continuous coverage of the In substrate, so that the signals from In and contamination present on its surface did not interfere with the NEXAFS spectra of the sample. Additionally, we used alternative methods for the sample preparation: Thin glycine films were cast on clean Au(111) wafers from saturated solutions of glycine in anhydrous trifluoroacetic acid (Gly/TFA), which has been used in previous NEXAFS studies of glycine,[12−15] and aqueous (ca. 70%) acetic acid (Gly/AcOH).

2.2. Sample Characterization with Powder X-ray Diffraction. Powder X-ray diffraction was applied to test the chemical identity, phase composition, and preferred orientation of crystallites in the glycine-related solid samples. The diffraction patterns were measured using an automatic powder diffractometer DRON-3 (Russia) equipped with a flat-crystal pyrolytic graphite monochromator in the Bragg−Brentano geometry with Cu Kα ($\lambda = 1.5418$ Å) radiation. The samples for the diffraction characterization were prepared similarly to the above two procedures applied for NEXAFS but using amorphous silica substrates instead of indium foil or gold wafers. To improve adhesion of the powder samples, the substrates were wetted with an inert solvent, hexane. The experimental diffraction patterns were compared with the theoretical ones calculated based on the literature crystallographic data for the respective phases and typical instrumental broadening parameters using the Crystallographica code.[24]

2.3. NEXAFS Data Collection. NEXAFS measurements were performed in an ultrahigh vacuum chamber installed at the bending magnet beamline HE-SGM of the synchrotron radiation facility BESSY II in Berlin. The NEXAFS spectra at the C, N, and O K-absorption edges were acquired in the partial electron yield mode with retardation voltages of −150 V (C K-edge), −300 V (N K-edge), and −350 V (O K-edge). The energy resolution of the setup is estimated at about 0.3 eV, slightly dependent on the photon energy. The scan steps were adjusted to 0.05 eV in the region of narrow spectral features and to 0.2−0.5 eV in the preedge and postedge regions. For most of the measurements, the incident beam was kept at the "magic angle" of 55°. Additionally, C K-edge NEXAFS spectra of pristine glycine powder film were measured under normal (90°) and grazing-incidence (20°) conditions. The raw NEXAFS spectra were corrected to the energy dependence of the incident photon flux by normalization to a spectrum of a freshly sputtered gold. For the absolute energy calibration of the C K-edge spectra, the simultaneously measured photoabsorption signal of a carbon-covered gold grid with a characteristic resonance at ∼285 eV was used. The position of this resonance was independently calibrated to the intense π^* peak of highly oriented pyrolytic graphite at 285.38 eV.[25] For the absolute energy calibration of the N and O K-edge NEXAFS spectra, we utilized the apparent shift in the position of the Au $4f_{7/2}$ core level of a clean Au on going from the beamline settings used for the C K-edge NEXAFS data collection to those for the N or O K-edges. We carefully checked that the experimental spectra were not affected by radiation damage effects. Even several successive spectra taken from the same place (as control measurements) did not exhibit any X-ray-induced changes above the normal statistical noise level. This is due to the moderate brilliance (i.e., the photon flux per illuminated area) provided by the bending magnet beamline HE SGM and optimized data acquisition time (about 2 min).

2.4. Theoretical Simulations of the NEXAFS Spectra. Polarization-averaged and polarization-dependent NEXAFS spectra of α-glycine at the C, N, and O K-edges were simulated using the cluster real-space multiple-scattering (RSMS) approach implemented in the FEFF8 code.[26−28] Crystallographic data for α-glycine reported in the literature[1] were used to generate the

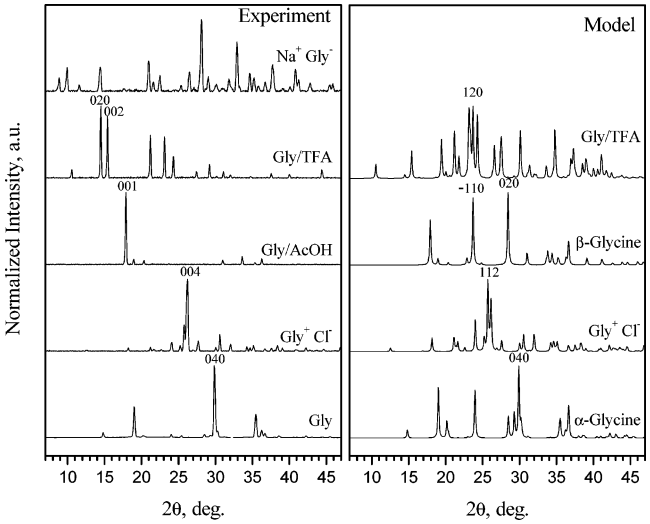

Figure 2. A comparison of the experimental X-ray diffraction patterns for the samples studied (left panel) and the model patterns calculated based on the crystallographic data for the respective reference phases (right panel). The *hkl* indices of the principle reflections in both patterns are marked.

input files. The scattering potential was calculated self-consistently for a sphere of 5.0 Å around the respective photoionized atom taking into account the presence of a dynamically screened 1*s* core hole. The full multiple-scattering (FMS) summation was applied to a sphere of 6.5 Å around the photoionized atom, and thus, the respective probe clusters contained about 150 atoms, i.e., a central molecule plus 14 neighboring molecules forming its proximate intermolecular environment. Atomic thermal vibrations were approximately taken into account within the correlated Debye−Einstein model by assigning a Debye−Waller factor of 0.01 Å^2 to all atoms in the probe cluster. In the cases of the carbon and oxygen spectra, partial contributions from nonequivalent atoms were calculated independently and totaled. FEFF outputs were consistently shifted by a few electronvolts to match the experimental energy scales.

3. Results and Discussion

3.1. X-ray Diffraction Characterization of the Samples. The experimental X-ray diffraction patterns of the studied samples were compared with simulations for the respective crystal phases in Figure 2. Pristine glycine proved to be strictly single-phase α-glycine (space group $P2_1/n$, $a = 5.10$, $b = 11.95$, $c = 5.46$ Å, $\beta = 111.78°$).[1] The powder after grinding comprises lamellar crystallites. The most intense line in the experimental pattern is 040 at ca. 29.9°, which indicates that the lamellae are most probably oriented preferably with the monoclinic axis *b* nearly normal to the surface of the powder films, i.e., along the *ac* plane. Note that it is the most typical morphology of α-glycine crystals since it is favored by the pattern of H-bonding formed by glycine zwitterions: the intermolecular H-bonds are the strongest in the *ac* plane.[1]

The experimental diffraction pattern of glycinium chloride is also fully consistent with the theoretical one (space group $P2_1/c$, $a = 7.12$, $b = 5.23$, $c = 13.75$ Å, $\beta = 97.25°$)[4] in terms of reflection positions, which implies the absence of admixture phases. The strongest experimental line is 004 at ca. 26.2°, which, coupled with the lamellar shape of the crystallites, indicates the preferred orientation along the *ab* plane. Again, it is exactly the morphology favored by the pattern of H-bonding.

Both solution-cast samples exhibit very strong preferred orientation. The film cast from concentrated aqueous acetic acid represents pure β-glycine (space group $P2_1$, $a = 5.09$, $b = 6.27$, $c = 5.38$ Å, $\beta = 113.19°$).[2] In this case, the crystallites are needle-shaped. The most intense line is 001 at ca. 17.9° assuming that the needles lying flat on the surface grow along the monoclinic *b* axis. Note that all reflections with a nonzero *k* (for instance, 020 at ca. 28.4°, which should be the most intense according to the simulation for an isotropically scattering powder) are strongly suppressed.

The film cast from anhydrous trifluoroacetic acid is single-phase glycinium trifluoroacetate (space group $P2_1/c$, $a = 4.96$, $b = 12.24$, $c = 12.02$ Å, $\beta = 106.67°$)[6] containing no crystallographic signature of pristine glycine. The crystallites have a shape of elongated prisms with the *a* axis parallel to the surface such that only 0*kl* reflections have significant intensity in the experimental pattern. The two most intense lines are 020 and 002 at ca. 14.5° and 15.4°, respectively. Reflections with a nonzero *h* (e.g., 120 at ca. 23.8°, which should be the strongest according to the simulation) are virtually completely suppressed.

The sodium glycinate sample is worth a special discussion. To our best knowledge, no lattice parameters for this phase were reported in the literature. The experimental pattern (see Figure 2) is complex but shows no evident admixtures of expectable foreign phases, such as three polymorphs of pristine glycine, sodium hydroxide/carbonates/hydrocarbonates, or their hydrates (sodium glycinate is typically produced by evaporation of aqueous solutions of equimolar mixtures of glycine and sodium hydroxide;[29] it is quite active toward CO_2 sorption and can readily convert into sodium carbonate and pristine glycine[30]). None of related metal glycinates matches the experimental pattern. Trial indexing of the pattern afforded the following parameters of a triclinic lattice: $a = 9.059(4)$, $b = 13.013(6)$, $c = 15.93(1)$ Å, $\alpha = 89.26(8)$, $\beta = 87.52(4)$, $\gamma = 79.37(2)°$ for 32 observed reflections with the discrepancies between the experimental and calculated positions not exceeding 0.04°. Quite similar parameters ($a = 10.44$, $b = 12.13$, $c = 15.04$ Å, $\alpha = 87.3$, $\beta = 89.6$, $\gamma = 62.2°$) were reported for a crystal of bis-(glycinato)zinc monohydrate, which appeared unsuitable for a detailed single-crystal X-ray diffraction study.[9] Taking into account the large unit volume (1844 Å^3), which means that the unit cell contains at least 16 formula units to provide realistic density, we suggest that the sodium glycinate sample represents a hydrate with a fractional amount of water (<1 H_2O molecule) per formula unit. We have no evidence that the sample is a mixture of phases. Apparently, the irregularly shaped flakelike crystallites do not show strong preferred orientation.

Therefore, the above X-ray diffraction elucidation indicates that all of the samples used are single-phase. Note that the two solution-cast glycine samples are significantly different. Casting from solutions of glycine in trifluoroacetic acid (Gly/TFA) results in glycinium trifluoroacetate, whereas casting from acetic solutions yields β-glycine.

3.2. The Experimental NEXAFS Spectra of Powder and Solution-Cast Glycine Films. The C, N, and O K-edge NEXAFS spectra of the powder film of pristine α-glycine (Gly) and of the glycine films cast from acetic (Gly/AcOH) and trifluoroacetic (Gly/TFA) acids are shown in Figure 3. The C K-edge spectra of pristine α-glycine as well as of Gly/AcOH and Gly/TFA (see left panel of Figure 3) manifest two weak preedge features at 285.2 and 287.3 eV (shoulder), a narrow resonance around 288.6 eV, and three broader resonances at ca. 291.5, 294.2, and 300.7 eV. Meanwhile, the spectrum of Gly/TFA shows some distinctions revealing extra features at

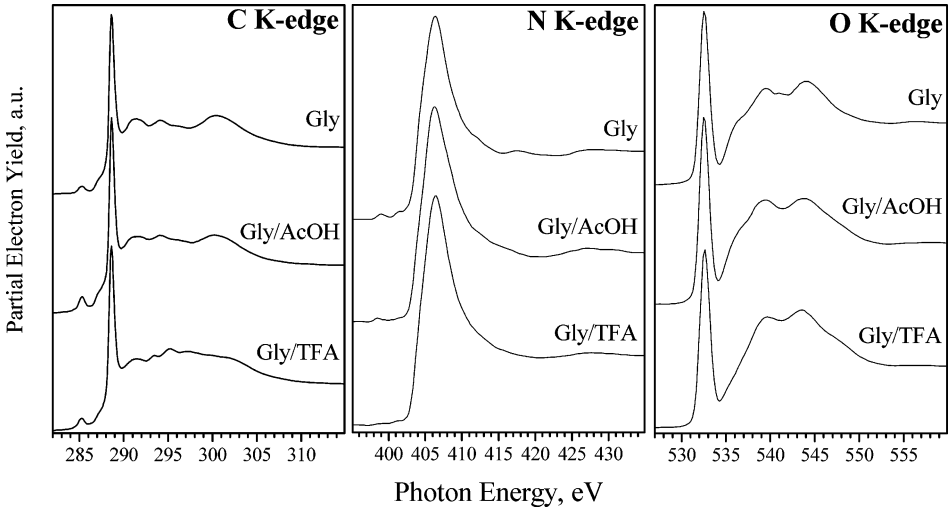

Figure 3. The C, N, and O (from left to right) K-edge NEXAFS spectra of the powder film of pristine glycine (Gly) and of thin films cast from solutions of glycine in acetic (Gly/AcOH) and trifluoroacetic (Gly/TFA) acids.

296−298 eV. This difference is attributable to the evident presence of trifluoroacetic acid in the sample: the respective features are observed in the gas-phase ISEELS spectrum of trifluoroacetic acid and can be assigned to the σ^*_{C-F} resonances of the CF_3 group.[13] The position of the main narrow resonance in all these samples lies in a narrow range of 288.60−288.65 eV.

The N K-edge NEXAFS spectra of the glycine samples shown in the central panel of Figure 3 are rather similar. The spectrum of glycine powder film reveals two rather weak preedge features at 398.9 and 401.4 eV (which are suppressed in the solution-cast films), the main resonance at 406.4 eV, and some diffuse postedge structure. The O K-edge NEXAFS spectra of the studied samples are shown in the right panel of Figure 3. Generally, the spectra reveal a strong narrow resonance at about 532.6 eV and a few broader postedge features at 535.8 (shoulder), 539.3, and 543.9 eV. The shoulder is especially pronounced in the spectra of glycine powder film and Gly/AcOH. In the case of Gly/TFA, the shoulder is nearly absent but the two other postedge peaks nearly converge into one broad maximum spanning over 540−543 eV.

The positions of observed spectral features in the C, N, and O K-edge NEXAFS spectra of the glycine powder film are summarized in Table 1. A suggestive assignment of the major spectral features will be given below based on theoretical simulations for zwitterionic α-glycine.

3.3. Theoretical Spectral Simulations for α-Glycine. Within the RSMS formalism, the C, N, and O K-edge NEXAFS spectra represent essentially the contributions of the partial 2p-electron densities of carbon, nitrogen, and oxygen atoms, respectively, into the total local density of states (LDOS) at the corresponding photoionized atom taking into account the presence of a dynamically screened 1s hole. The NEXAFS spectrum is calculated by adding a steplike atomic absorption background to the respective element- and orbital moment-projected LDOS broadened to account for the finite lifetime of the core hole.[26,27] To make traditional assignment of the NEXAFS spectral features to specific electronic transitions, such as C 1s → σ^*_{C-N} or $\pi^*_{C=O}$, in the theoretical spectra calculated in this way, we utilized the following procedure. The spectra calculated for all non-hydrogen atoms constituting the glycine molecule were put into the common energy scale by subtracting the ionization potentials (IP) of the respective core levels (which, within the RSMS formalism, correspond to the muffin-tin zeros) from the "as calculated" photon energy values. A spectral feature that appears in calculated partial contributions from two or more different atoms at the same position should thus be assigned to an antibonding orbital delocalized over these atoms. To differentiate between σ^* and π^* orbitals, we calculated the polarization-averaged and polarization-dependent spectra for different polarization directions relative to the glycine molecule. The σ^*-type features should be maximized in intensity when the polarization is directed parallel to the respective bond. In contrast, the π^*-type features should be maximized in intensity when the polarization is perpendicular to the respective bond. Since four out of five non-hydrogen atoms of the glycine molecule (except for nitrogen) lie virtually in one plane, the *x* and *y* axes of the coordinate system were selected in this plane, the *x* axis being parallel to the C−C bond, as shown at the top of Figure 4. The *z* axis was perpendicular to the plane. In this coordinate system, π^* components should be most prominent for the polarization direction p || *z*, whereas the σ^*_{C-C} component should be the maximum for the polarization direction p || *x* and nearly absent for p || *z* and p || *y*, and so on.

The theoretical NEXAFS spectra of four chemically non-equivalent non-hydrogen atoms (for simplicity, the two oxygen

TABLE 1: Positions of the Main Spectral Features for the Glycine-Related Samples Studied[a]

sample	edge	positions of the spectral features, eV[b]
Gly	C	285.2, 287.3 (sh), 288.6, 291.5, 294.2, 300.7
	N	398.9, 401.4, 406.4, 412.2 (sh), 417.3
	O	532.6, 535.8 (sh), 539.3, 543.9
Gly′	C	285.2, 287.3 (sh), 288.6, 291.5, 294.2, 300.7
	N	399.4, 401.2, 406.0, 412.2 (sh), 417.3
	O	532.5, 535.8 (sh), 538.7, 543.5
Gly″	C	285.2, 287.3 (sh), 288.5, 291.5, 294.2, 300.7
	N	400.9, 406.0, 412.2, 417.3
	O	532.4, 535.8 (sh), 538.8, 543.8
$Gly^+ Cl^-$	C	285.2, 287.3 (sh), 288.6, 291.4, 294.7, 299.6, 301.6 (sh)
	N	406.4
	O	532.5, 540.4, 543.2
Na^+ Gly	C	285.2, 287.3 (sh), 288.6, 289.9, 292.1, 295.2, 299.8
	N	398.6, 402.4, 405.6, 413.4
	O	532.7, 535.8 (sh), 540.4, 543.5

[a] For a suggestive assignment of the features for pristine glycine, see text. [b] The accuracy in determined positions of distinct narrow preedge features is estimated to ±0.1 eV; the accuracy in determined positions of shoulder peaks denoted as (sh) and broad postedge features are estimated to ±0.25 eV.

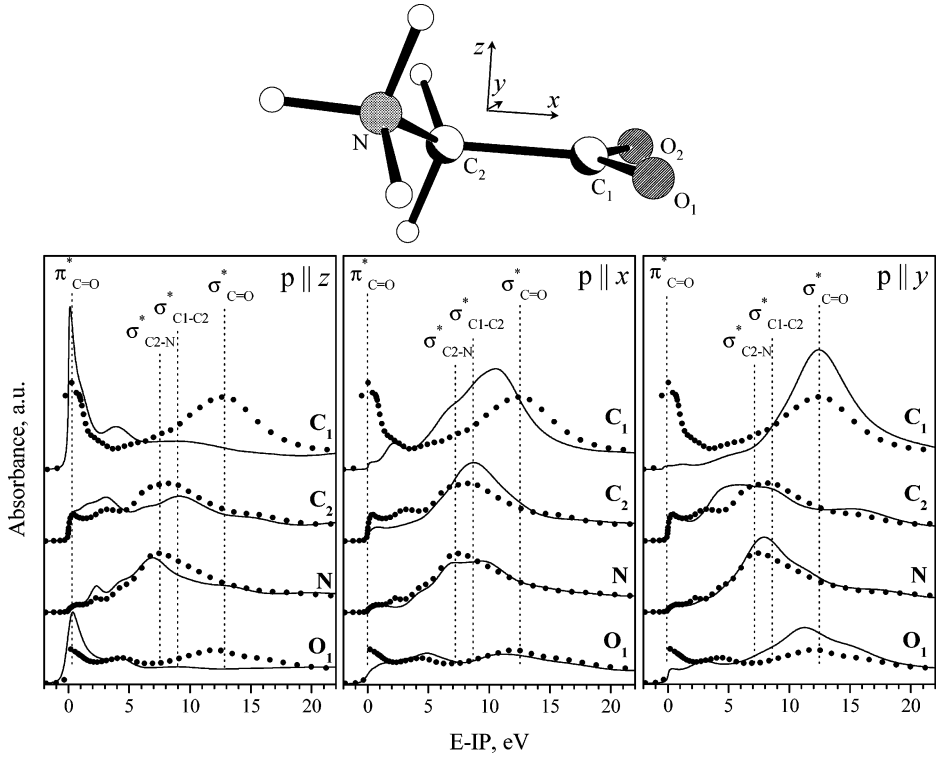

Figure 4. The theoretical polarization averaged (circles) and polarization-dependent (solid lines) NEXAFS spectra of α-glycine at the C, N, and O K-edges (put into the common energy scale as described in the text) for three different polarization directions. The coordinate system associated with the glycine molecule is shown at the top.

atoms are for the moment considered to be identical) simulated on the basis of crystallographic data for α-glycine[1] are shown in Figure 4. On the basis of the formal approach described above, four major spectral features can easily be identified. They are: $\pi^*_{C=O}$ at ∼0.4 eV, which dominates the calculated spectra of C_1 and O_1 for p || *z*; σ^*_{C2-N} at ∼7.5 eV, which is manifested in the spectra of C_2 and N for all three polarization directions with comparable intensities; σ^*_{C1-C2} at ∼9.0 eV, which is characterized by the highest intensity in the spectra of C_1 and C_2 for p || *x*; and $\sigma^*_{C=O}$ at ∼12.9 eV, which is most prominent in the calculated spectra of C_1 and O_1 for p || *y*. It has to be noted that the extent of the linear dichroism, i.e., the difference between the spectra calculated for different polarization directions, is the largest for the carboxylate carbon atom C_1; for the polarization direction p || *z*, it manifests a very intense $\pi^*_{C=O}$ peak and a flat low-intensity signal in the region of the $\sigma^*_{C=O}$ feature, while the situation is reversed for the polarization directions p || *x* and p || *y*. The analogous dichroism is observed for O_1, but its extent is smaller in this case. Additionally, the C_1 and O_1 atoms manifest a rather weak broad peak in a range of 3−5 eV, which is prominent for p || *z* and p || *x*. Surprisingly, the calculated spectra of C_2 and N also reveal some intensity in the region of 0−5 eV with the weak polarization dependence. This contradicts to the simple building-block picture, which predicts only σ^* (i.e., C−C, C−N, C−H, and N−H) components for these two atoms. We attribute these spectral features to a minor contribution of the aminic carbon and nitrogen atoms to the carboxylate π-system of the glycine molecule. We speculate that the π-delocalization is partially intermolecular (rather than purely intramolecular) due to the extended network of H-bonds, so that the orientation of the respective transition dipole moment strictly perpendicular to the plane of bonds is somewhat violated. Likely, electronic transitions derived from hydrogen atoms and low-lying Rydberg states of the carbon and nitrogen atoms also contribute to this spectral region. Unfortunately, contributions involving H atoms (i.e., $\sigma^*_{C_2-H}$ and σ^*_{N-H}) cannot be unequivocally identified using the procedure applied.

The calculated polarization-averaged NEXAFS spectra of zwitterionic α-glycine are compared with the magic-angle experimental spectra in Figure 5. Overall, the correspondence between the simulated and experimental C K-edge NEXAFS spectra (see left panel of Figure 5) is fair; all the main features observed in the experimental spectrum are reasonably reproduced. The aforementioned π^*- and Rydberg-state-derived features of the aminic carbon atom C_2 are responsible for the weak preedge peaks between 285 and 287 eV (note that the ionization potential of C_2 is lower than that of C_1 by about 3 eV, i.e., 285 and 288 eV, respectively). The main resonance at 288.6 eV is naturally attributed to the $\pi^*_{C=O}$ component. The two-peak structure at 291−295 eV is mainly due to overlapped contributions from the $\sigma^*_{C_2-N}$ and $\sigma^*_{C_1-C_2}$ components. The broad peak at 307 eV can be reliably assigned to the $\sigma^*_{C=O}$ feature. Note that except for the very first preedge features, the above assignment is fully consistent with that proposed by other authors based on calculations utilizing the direct molecular representation for an isolated glycine molecule.[13,23] The simulated N K-edge spectrum of zwitterionic α-glycine demostrates remarkable similarity to the experimental spectrum (see central panel of Figure 5). The major maximum is dominated by the $\sigma^*_{C_2-N}$ component. The origin of the two weak preedge peaks in the N K-edge experimental spectrum is fully analogous to those in the C K-edge spectrum discussed above. Their intensity is apparently overestimated by the simulation.

Two oxygen atoms of zwitterionic glycine are equivalent chemically but experience slightly different intermolecular environments.[1] Correspondingly, the two simulated spectra are quite similar (see right panel of Figure 5) although not completely identical. The simulated spectra manifest two major features at ca. 532 and 544 eV, which represent the oxygen

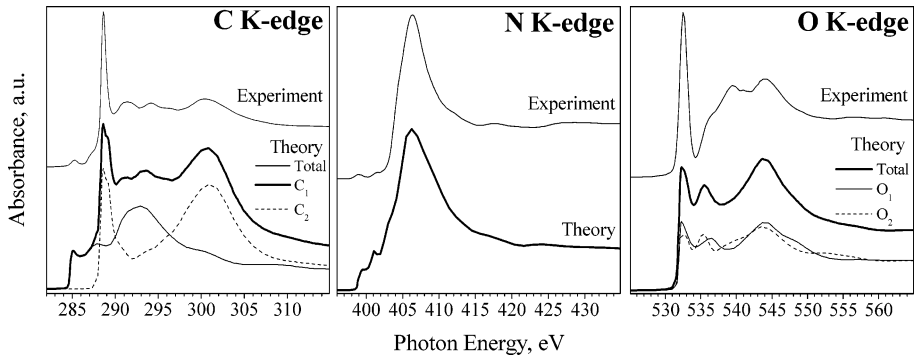

Figure 5. Comparison of the experimental NEXAFS spectra of pristine glycine at the C, N, and O K-edges with the corresponding calculated polarization-averaged NEXAFS spectra of zwitterionic α-glycine. The theoretical spectra are FEFF outputs shifted by 3.35, −0.50, 1.00, 3.25, and 3.00 eV for C_1, C_2, N, O_1, and O_2, respectively.

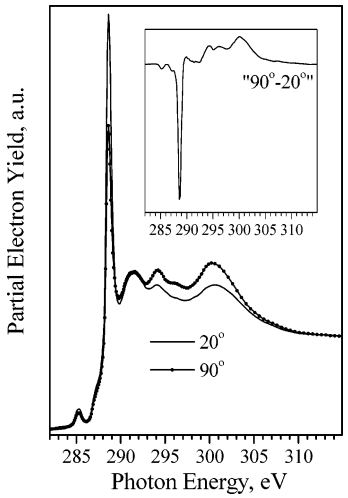

Figure 6. Linear dichroism in the C K-edge spectra of the powder film of pristine glycine.

counterparts of the aforementioned features at 288.6 and 300.7 eV observed in the C K-edge spectra, i.e., they can be ascribed as $\pi^*_{C=O}$ and $\sigma^*_{C=O}$, respectively. Although these spectral features also occur in the experimental spectrum, there is a serious discrepancy between the simulation and the experiment. The experimental spectrum shows a prominent peak at ca. 539 eV (see Table 1), whereas the simulation lacks intensity in this region. This implies either deficiency of the theoretical approach or the presence of extra oxygen atoms in the sample, which are not accounted for by the simulation. A possible source of such additional oxygen atoms is a minute contamination of the hydrophilic glycine samples with chemisorbed water. In particular, O K-edge NEXAFS spectra of mixed glycine/ice films prepared by codeposition under ultrahigh vacuum conditions are dominated by a broad maximum at 537−542 eV.[32] The O K-edge spectrum of aqueous solution of glycine reported by Messer et al.[23] also looks similar.

3.4. Polarization Dependence and Reproducibility of the NEXAFS Spectra of Glycine. According to powder X-ray diffraction data discussed in section 3.1, the pristine glycine powder manifests texture preferably exposing [010] planes. To examine the effects of this texture in the NEXAFS spectra and verify the above assignment of the NEXAFS spectral features based on the theoretical simulations, we measured the C K-edge spectra at normal (90°) and grazing (20°) incidense with respect to the surface of the powder film sample. The respective spectra as well as their difference "90° − 20°" are shown in Figure 6. The difference between the spectra due to the linear dichroism effects is apparent. The intensity of the dominant $\pi^*_{C=O}$ resonance is reduced by more than 25% on going from grazing incidense to normal incidense geometry. Respectively, the intensity of the $\sigma^*_{C_1-C_2}$ and $\sigma^*_{C=O}$ features is noticeably enhanced. It is of note that the weak preedges and the feature at 291.5 eV mostly formed by the $\sigma^*_{C_2-N}$ component reveal no strong polarization dependence. These results are fully consistent with the expected preferred orientation of glycine molecules with the plane defined by the carboxylate group and the C_1-C_2 bond parallel to the sample surface.

As a result of several independent NEXAFS measurements on nominally identically prepared powder films of pristine glycine, we noticed some correlated variations in the spectra, which were especially prominent at the nitrogen K-edge. The C, N, and O K-edge spectra of three representative examples of similarly prepared glycine samples, viz., Gly, Gly′, and Gly″, are shown in Figure 7. A few of the measured glycine samples manifested in their N K-edge spectra a relatively intense preedge feature at 400.9 eV (as in Gly″, see central panel of Figure 7, this spectrum was reported in our previous study[21]); other samples revealed two weaker preedge features at 399.4 and 401.2 eV (as observed for Gly′). Nevertheless, the spectra with only a hint of the above preedge peaks (as in Gly) occurred most frequently and reproducibly. It is of note that the occurrence of the preedge resonances correlates with the position of the main absorption maximum (which shifts from ca. 406.0 eV in Gly″ and Gly′ to ∼406.4 eV in Gly), its intensity (the larger the integral area under the preedge peaks, the lower the intensity of the main peak), and intensity of the postedge features at ca. 412.2 and 417.3 eV. Additionally, in the case of Gly″, the intensities of both the π^* and σ^* spectral features in the C K-edge spectra (see left panel of Figure 7) are simultaneously reduced (which thus cannot be explained by linear dichroism effects due to a preferred orientation) and the $\pi^*_{C=O}$ resonance is noticeably broadened and shifted to 288.50 eV.[21] The oxygen K-edge spectra also show some variations, mostly in the region 537−542 eV, which was tentatively assigned above to spurious adsorbed water. To rationalize the observed differences between the spectra of similarly prepared pristine glycine samples, a number of factors can be proposed. First, the amount of coadsorbed water, which primarily affects the O K-edge spectra, is naturally dependent on such difficult-to-control factors as humidity of ambient or duration of pumping. The coadsorbed water molecules would form strong H-bonds with glycine molecules disturbing their intermolecular environment. Second, an alteration of the charge state of zwitterionic glycine molecules or long-range crystalline order in the near-surface regions, which is actually probed with the partial electron yield NEXAFS acquisition mode, cannot be totally ruled out. Although neutral glycine is thermodynamically stable only in the gas phase, it

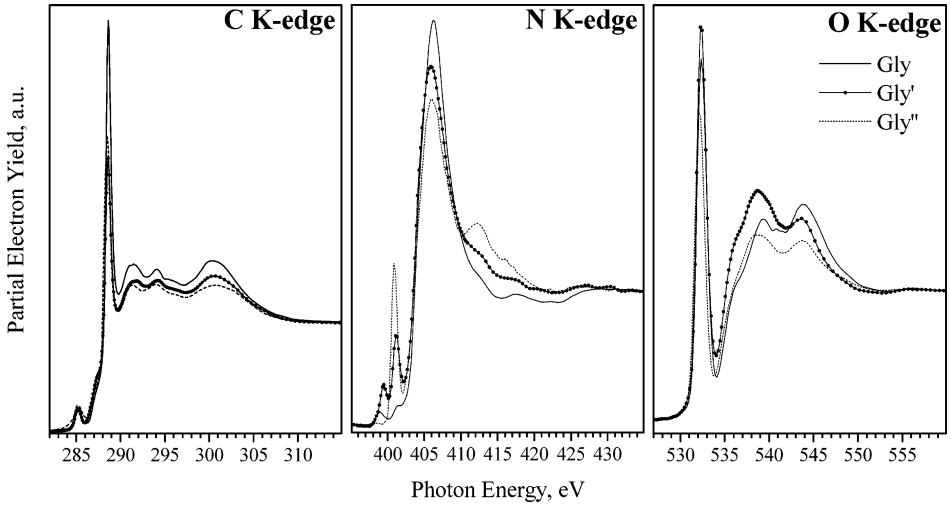

Figure 7. Variations in the C, N, and O K-edge NEXAFS spectra of nominally identically prepared samples of pristine glycine.

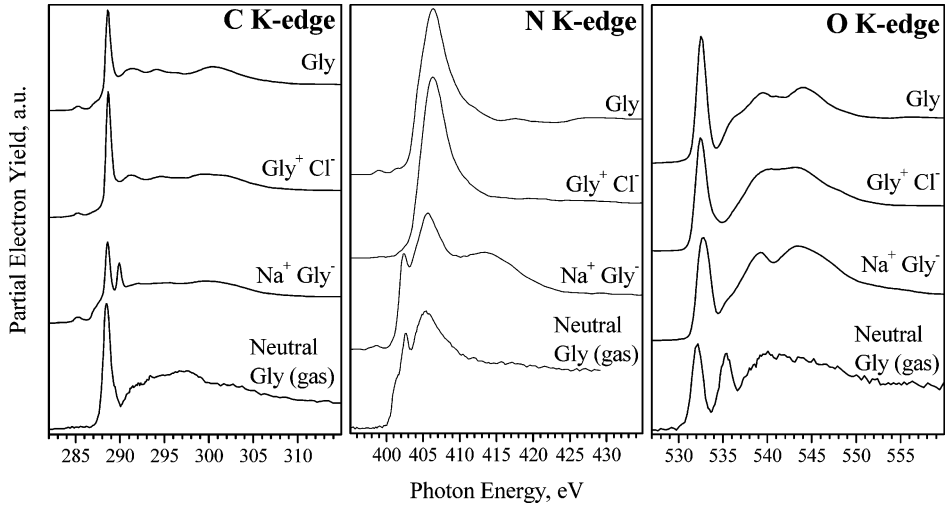

Figure 8. Comparison of the C, N, and O (from left to right) K-edge NEXAFS spectra of glycine in various charge states: zwitterionic α-glycine, glycinium chloride, sodium glycinate, and neutral glycine (the gas-phase ISEELS spectra[14,15,31]).

can occur in solid phases as a kinetically stabilized metastable state. For instance, it was detected in the bulk of vacuum-deposited films of glycine at low temperatures.[33] Probably, neutral glycine molecules can also occur at interfaces or defect sites when intermolecular bonds of a glycine molecule with its neighbors are substantially weakened. Therefore, the fraction of neutral molecules in a sample can vary as a function, for instance, of the mean particle size or concentration of defects introduced by grinding of the polycrystalline powder. Alternatively, grinding can initiate some chemical reactions with glycine, such as polycondensation giving rise to oligopeptides or 3,5-diketopiperazine. X-ray diffraction data show that α-glycine readily undergoes amorphization upon intense grinding. Therefore, we attribute these spectral variations either to mechanochemical damage of α-glycine upon grinding (in the case of Gly″) or variations in the amount of coadsorbed water (in the case of Gly′).

3.5. The Experimental NEXAFS Spectra of Glycinium Chloride and Sodium Glycinate. The NEXAFS spectra of the ionic salts of glycine, viz., $Gly^+ Cl^-$ and $Na^+ Gly^-$ at the C, N, and O K-edges are compared in Figure 8 with the respective spectra of pristine glycine and with the ISEELS spectra of neutral gaseous glycine retrieved from the Database of Inner-shell Excitation Spectra of Gas-Phase Atoms and Molecules[14,15,31] compiled by A. P. Hitchcock et al. at the McMaster University, Hamilton, Canada. The C K-edge spectrum of $Gly^+ Cl^-$ looks rather similar (see left panel of Figure 8) to that of pristine glycine, but the high-lying $\sigma^*_{C=O}$ resonance is somewhat broadened and its apparent maximum is shifted to 299.6 eV (see Table 1). Meanwhile, the spectrum of $Na^+ Gly^-$ is distinctly different exhibiting the second narrow resonance at 289.9 eV and smeared postedge structure at 292−300 eV. Note that the position of the main $\pi^*_{C=O}$ resonance remains unaltered within the experimental accuracy over the three studied samples. This is in some contradiction to the results reported by Messer et al.[23] for aqueous solutions of glycine at different pH. They observed a shift of the $\pi^*_{C=O}$ resonance by 0.2 eV to lower energies on going from the glycinate anion to glycinium cation.

Similarly, we observe no dramatic difference between zwitterionic pristine glycine and glycinium chloride in the N K-edge spectra (see central panel of Figure 8) although weak preedge features observed in the spectrum of Gly are virtually completely suppressed in the case of $Gly^+ Cl^-$. It is of note that the latter spectrum is nearly undistinguishable from that of Gly/TFA (see Figure 3), which is not surprising since this sample also comprises glycinium cation and the N K-edge spectrum is not affected by the presence of trifluoroacetate. In contrast, the N K-edge spectrum of sodium glycinate is substantially different from those of both zwitterionic glycine and glycinium cation (see central panel of Figure 8). It exhibits two preedge features (a weak peak one at 398.6 eV and a rather strong feature at 402.4 eV), the main peak located at 405.6 eV and a prominent

broad postedge peak centered at 413.4 eV (see Table 1). Following the formal algorithm utilized in the analysis of the theoretical spectra of α-glycine performed in section 3.3, it can be suggested that the new narrow resonances observed in the C and N K-edge NEXAFS spectra of Na^+ Gly^- are of a common origin, since they occur at similar positions for the C_1 and N atoms when the spectra are put into the common scale (i.e., ∼2.0 eV). Probably, they arise due to the appearance of a new low-lying weakly antibonding state with contributions of the C_1, N, and, probably, Na atoms. It has to be mentioned that Messer et al.[23] also reported the emergence of an intense preedge peak in the N K-edge spectra of alkaline glycine solutions at a position close to the position of strong preedge peak observed in the spectrum of neutral gaseous glycine and attributed to transitions to 3p Rydberg states, which are thus expected to be quenched in the solid state.[14,15] In our case, the N K-edge spectrum of solid Na^+ Gly^- also bears some resemblance to that of neutral glycine as regards position of the preedge peak and the shape of the main resonance but the two spectra are distinctly different in the postedge region, which thus has to be attributed to effects of the intermolecular environment.

There are also some differences between the three studied samples in the O K-edge spectra, which mostly relate to the shape of postedge σ^* features, whereas the position of the dominant $\pi^*_{C=O}$ resonance remains constant within the experimental accuracy (in contrast to the shift by 0.25 eV to lower energies for the glycinium cation reported by Messer et al.[23]). Unfortunately, the observed differences in the σ^* region cannot be conclusively analyzed due to the probable effects of water admixtures.

4. Conclusions

The experimental NEXAFS spectra of glycinate anion at the C and N K-edges manifest substantial differences from those of zwitterionic α-glycine, β-glycine, and glycinium cation, whereas the spectra of the three latter forms are rather similar. The four major features, i.e., π^*_{COO}, σ^*_{COO}, σ^*_{C-C}, and σ^*_{C-N}, are objectively identified in the NEXAFS spectra of pristine α-glycine based on the theoretical simulations. The weak preedge features observed in the C and N K-edge NEXAFS spectra of pristine glycine are tentatively assigned to the partial involvement of the aminic carbon and nitrogen atoms into the π-system of glycine due to intra- and intermolecular delocalization.

Acknowledgment. We are grateful to Professor A. Ankudinov and Professor J. Rehr (University of Washington, Seattle) for the FEFF8 code, Ch. Wöll (Universität Bochum) for providing us with the experimental equipment at BESSY II, and the BESSY staff for their technical support during beamtime. This work was supported by the German BMBF (Project No. 05 KS4VHA/4, 05 KS4WWA/6, and 05 ES3XBA/5), the Russian Foundation for Basic Research (Grant 05-03-32871a), Fonds der Chemischen Industrie (M.G.), and the Office of Naval Research (Y.Z.).

Supporting Information Available: FEFF8 input files containing the control cards and atomic coordinates used to generate the theoretical spectra reported together with some additional computational details. This material is available free of charge via the Internet at http://pubs.acs.org.

References and Notes

(1) Langan, P.; Mason, S. A.; Myles, D.; Schoenborn, B. P. *Acta Crystallogr.* **2002**, *B58*, 728.

(2) Drebushchak, T. N.; Boldyreva, E. V.; Shutova, E. S., *Acta Crystallogr.* **2002**, *E58*, o634.

(3) Kvick, Å. *Acta Crystallogr.* **1980**, *B36*, 115.

(4) Al-Karaghouli, A. R.; Cole, F. E.; Lehmann, M. S.; Miskell, C. F.; Verbist, J. J.; Koetzle, T. F. *J. Chem. Phys.* **1975**, *63*, 1360.

(5) Cherouana, A.; Benali-Cherif, N.; Bendjeddou, L.; Merazig, H. *Acta Crystallogr.* **2002**, *E58*, o1351.

(6) Rodrigues, V. H.; Paixão, J. A.; Costa, M. M. R. R.; Beja, A. M. *Acta Crystallogr.* **2002**, *C58*, o658.

(7) Nandhini, M. S.; Krishnakumar, R. V.; Natarajan, S. *Acta Crystallogr.* **2001**, *C57*, 116.

(8) Acland, C. B.; Freeman, H. C. *J. Chem. Soc. D, Chem. Commun.* **1971**, *17*, 1016.

(9) Low, B. W.; Hirshfeld, F. L.; Richards, F. M. *J. Am. Chem. Soc.* **1959**, *81*, 4412.

(10) Muller, G.; Maier, G.-M.; Lutz, M. *Inorg. Chim. Acta* **1994**, *218*, 121.

(11) Stöhr, J. *NEXAFS Spectroscopy*; Springer-Verlag: Berlin, 1992.

(12) Boese, J.; Osanna, A.; Jacobsen, C.; Kirz, J. *J. Electron Spectrosc.* **1997**, *85*, 9.

(13) Kaznacheyev, K.; Osanna, A.; Jacobsen, C.; Plashkevych, O.; Vahtras, O.; Ågren, H.; Carravetta, V.; Hitchcock, A. P. *J. Phys. Chem. A* **2002**, *106*, 3153.

(14) Gordon, M. L.; Cooper, G.; Morin, C.; Araki, T.; Turci, C. C.; Kaznatcheev, K.; Hitchcock, A. P. *J. Phys. Chem. A* **2003**, *107*, 6144.

(15) Cooper, G.; Gordon, M.; Tulumello, D.; Turci, C.; Kaznatcheev, K.; Hitchcock, A. P. *J. Electron Spectrosc.* **2004**, *137*−*140*, 795.

(16) Hasselström, J.; Karis, O.; Weinelt, M.; Wassdahl, N.; Nilsson, A.; Nyberg, M.; Pettersson, L. G. M.; Samant, M. G.; Stöhr, J. *Surf. Sci.* **1998**, *407*, 221.

(17) Nyberg, M.; Hasselström, J.; Karis, O.; Wassdahl, N.; Weinelt, M.; Nilsson, A.; Pettersson, L. G. M. *J. Chem. Phys.* **2000**, *112*, 5420.

(18) Nyberg, M.; Odelius, M.; Nilsson, A.; Pettersson, L. G. M. *J. Chem. Phys.* **2003**, *119*, 12577.

(19) Tzvetkov, G.; Koller, G.; Zubavichus, Y.; Fuchs, O.; Casu, M. B.; Heske, C.; Umbach, E.; Grunze, M.; Ramsey, M. G.; Netzer, F. P. *Langmuir* **2004**, *20*, 10551.

(20) Tanaka, M.; Nakagawa, K.; Koketsu, T.; Agui, A.; Yaokoya, A. *J. Synchrotron Rad.* **2001**, *8*, 1009.

(21) Zubavichus, Y.; Zharnikov, M.; Schaporenko, A.; Grunze, M. *J. Electron Spectrosc.* **2004**, *134*, 25.

(22) Zubavichus, Y.; Schaporenko, A.; Grunze, M.; Zharnikov, M. *J. Phys. Chem. A* **2005**, 109, 6998.

(23) Messer, B. M.; Cappa, C. D.; Smith, J. D.; Wilson, K. R.; Gilles, M. K.; Cohen, R. C.; Saykally, R. J. *J. Phys. Chem. B* **2005**, *109*, 5375.

(24) Crystallographica v.1.22, Oxford Cryosystems, 1995−1997; http://www.crystallographica.com.

(25) Batson, P. E. *Phys. Rev. B* **1993**, *48*, 2608.

(26) Rehr, J. J.; Albers, R. C.; Zabinsky, S. I. *Phys. Rev. Lett.* **1992**, *69*, 3397.

(27) Ankudinov, A. L.; Ravel, B.; Rehr, J. J.; Conradson, S. D. *Phys. Rev. B* **1998**, *58*, 7565.

(28) Rehr, J. J.; Ankudinov, A. L. *Coord. Chem. Rev.* **2005**, *249*, 131.

(29) Lian, Y.; Kingman, N. G. *J. Pharm. Sci.* **2002**, *91*, 2367.

(30) Chen, H.; Kovvali, A. S.; Sirkar, K. K. *Ind. Eng. Chem. Res.* **2000**, *39*, 2447.

(31) Hitchcock, A. P.; Mancini, D. C. *J. Electron Spectrosc.* **1994**, *67*, 1.

(32) Tzvetkov, G.; Zubavichus, Y.; Koller, G.; Fuchs, O.; Heske, C.; Umbach, E.; Grunze, M.; Ramsey, M. G.; Netzer, F. P. *BESSY Jahresbericht* **2002**, 183.

(33) Gomez-Zavaglia, A.; Fausto, R. *Phys. Chem. Chem. Phys.* **2003**, *5*, 3154.